Statistical and pre-equilibrium (γ,α) cross sections of ^{90}Zr and their multipolarities via the ^{90}Zr(e,α) reaction

T. Tamae,* T. Urano, M. Hirooka, and M. Sugawara

Laboratory of Nuclear Science, Tohoku University, Mikamine, Sendai, Japan

The (e,α) cross section in ^{90}Zr has been measured at incident electron energies from 13.5 MeV to 66.5 MeV for α particles between 6.9 and 16.8 MeV. The (γ,α) cross section was deduced from it assuming both $E1$ interaction and $E2$ interaction. The angular distribution of the (γ,α_0) cross section and an experiment using the bremsstrahlung plus electron beam make it clear that the $E1$ interaction is dominant over all the present energy range. The (γ,α) cross section extracted by using $E1$ virtual photon spectra has a large bump above the excitation energy of 30 MeV in addition to a bump in the giant dipole resonance region. The (γ,α_0) cross section also has a bump at the giant dipole resonance which exhausts most of the (γ,α) cross section in that region. The compound nucleus model was used successfully to explain the bump at the giant dipole resonance. The cross section above 30 MeV is discussed in terms of the pre-equilibrium α emission process combined with the quasi-deuteron model.

NUCLEAR REACTIONS ^{90}Zr(e,α), $E_e = 13.5$–66.5 MeV; measured $d\sigma(e,\alpha)/d\Omega$, deduced $d\sigma(\gamma,\alpha)/d\Omega$ and $d\sigma(\gamma,\alpha_0)/d\Omega$. Angular distributions; (γ,α_0) at $E_e = 17.5$ MeV and (e,α) at $E_e = 40.0$ MeV, $\theta_\alpha = 45$–135°. Experiment using electron plus bremsstrahlung at $E_e = 60.0$ MeV. Calculations, compound nucleus model, and pre-equilibrium exciton model combined with quasi-deuteron model.

I. INTRODUCTION

A number of studies have been made of alpha spectra in (γ, α) reactions on medium-weight nuclei.[1-9] Most cases have been explained quite well by statistical model calculations. In heavy nuclei such as In and Au, however, an excess of energetic α particles has been observed in comparison with those expected from the evaporation model.[5] Isotropic angular distributions were obtained for α particles with low energies in ^{63}Cu and Zn as expected by the statistical model.[9,10] On the other hand, α particles from heavier nuclei showed a strong forward peaking, which suggested a direct process.[9,11] Forward-peaked angular distributions were measured for the high energy component of α particles even in ^{60}Ni and ^{63}Cu (Refs. 11 and 12). The measurements of Flowers *et al.* showed that the high energy α particles exhibit a cross section in ^{60}Ni several orders of magnitude above the statistical model prediction,[12] and they suggested that the two-step process involving (γ,N) and (N,α) reactions might explain these experimental results [the symbol N means a nucleon (neutron or proton)].

In regard to the emission of an α particle from heavy nuclei, studies of the (n,α) and (p,α) reactions also have been carried out successfully in the framework of the pre-equilibrium exciton model, in which a performed α particle is emitted in the intranuclear cascade mechanism.[13-16]

The photonuclear reaction in the high energy region has been studied mainly on the basis of the quasi-deuteron model discussed by Levinger.[17] In the region above 150 MeV, the model has successfully predicted the production cross sections for high energy nucleons, energy and angular distributions of outgoing nucleons, as well as the presence of neutron-proton coincidences.[18-22] Also in the region under 150 MeV, several investigations have been made in the framework of this model,[23,24] and attempts have been made to take account of the scattering and reabsorption of the emerging nucleons by the target nucleus.[25-28] The intranuclear cascade model and the pre-equilibrium exciton model have been combined with the quasi-deuteron model to interpret photonuclear reactions above the giant resonance.[27,29,30]

The (γ, α) reaction on heavy nuclei is suitable for the study of the photonuclear reaction in the high energy region because α emission through the giant resonance is suppressed by the high Coulomb barrier. However, only a few such cross sections have been measured as a function of excitation energy, and there is little information on the reaction mechanism above the giant resonance region. In the giant resonance region, the (γ, α_0) and (α,γ_0) reactions have been studied on several nuclei lighter than the Ni isotopes.[31-36] The angular distributions of (γ, α_0) cross sections in such nuclei show that the $E2$ component is less than 10%

of the E1 cross section. Recently Wolynec *et al.*
have measured the (e,α) cross sections in the Ni
isotopes up to 50 MeV and suggested a large E2
cross section should exist in the isoscalar giant
quadrupole resonance (GQR) region.[37] They claimed
that electroproduced α particles decay preferenti-
ally to the 2^+ first excited state. However, more
work needs to be done in order to understand the
reaction mechanism of the photoalpha reaction in
this region. Moreover, the E2 contribution is un-
certain in heavier nuclei and in the region above
the giant resonance. It is important to understand
correctly the contribution of the E2 interaction
in these cases.

This paper presents measurements of the
$^{90}Zr(\gamma,\alpha)$ cross section up to 60 MeV, and gives
the multipolarity for the cross section by means
of an experiment using bremsstrahlung plus elec-
trons. Angular distributions are given both for
the (γ,α_0) and (e,α) reactions.

Also, the results of two kinds of calculation, the
compound nucleus model and the pre-equilibrium
exciton model combined with the quasi-deuteron mo-
del, are compared with the experimental cross
sections.

II. EXPERIMENTAL PROCEDURES

The experiments were performed with electron
beams from the Tohoku University electron Linac.
An enriched ^{90}Zr target, of 97.80% purity and
5.08 mg/cm^2 thickness, was bombarded with elec-
trons, whose energy resolution was fixed at 2.0%.
Electron beam currents were monitored with a
ferrite core monitor calibrated with an accuracy
of 1%. Alpha particles were detected with a multi-
wire proportional counter (MWPC) placed in the
focal plane of a Browne-Büechener type broad
range spectrometer.[38] The window of the MWPC
is a 644 mm long and 30 mm wide aluminized
Mylar sheet 12 μm thick, which is reinforced
outside with 4 mm tungsten meshes of 200 μm
diameter. A hundred sense wires made of 30 μm
diameter gold-plated tungsten were stretched
6 mm apart providing energy and position resolu-
tions of 0.6% and 3 mm respectively measured
vertically to the direction of the particle orbits.
The distance between the sense wire plane and
cathode plane is 5 mm. High voltage of 1.2 kV
was supplied to the sense wires and signals were
taken out through capacitors. PR gas (90% Ar,
10% CH$_4$) at atmospheric pressure was used as
the counter gas at a flow rate of 15-35 cm^3 per
minute. Cards of charge-sensitive pre-amplifiers
were attached directly to the chamber frame.

A set of signals on several successive wires is
made by one incident particle as shown in Fig. 1
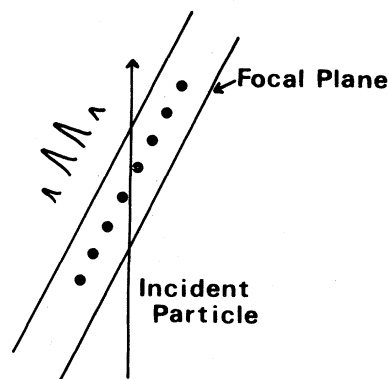
FIG. 1. An incident particle passes obliquely through
the MWPC and makes signals on several successive
wires.

because its track is inclined to the MWPC at an
acute angle (21.50°-37.52°). An electronics sys-
tem identifies the signals as due to one particle.
The entrance window plane of the MWPC is located
in the focal plane, so that an incident particle in-
tersects the focal plane at the point of the first
wire of the successive wires which produce sig-
nals. The measurement of the sum of their pulse
heights, which is proportional to the energy loss
of the incident particle in the counter gas, allows
particle identification.

Figure 2 shows the schematic diagram of the
data acquisition system. It delivers the sum of
pulse heights on the successive wires and the
wire number of the first wire to the computer.

Figure 3 shows pulse height spectra from the
MWPC. A discrimination level was set at an inter-
mediate point of α particles and tritons. The
pulse height of α particles is 10 times as large as
that of protons, and can be discriminated from the
proton background. Yields of deuterons, tritons,
and ^3He particles are very small in medium-
weight nuclei, and the background from them can
be ignored.

An example of an α-particle energy spectrum is
shown in Fig. 4. This was corrected for energy
loss on the assumption that each α particle orig-
inated half-way through the target. The energy
loss is about 0.7 MeV at α energy of 10 MeV. The
experimental conditions are shown in Table I.
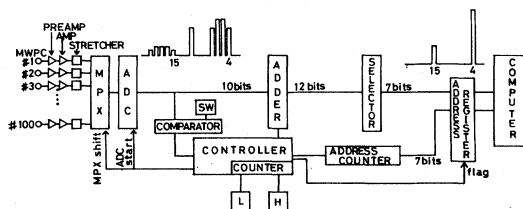
FIG. 2. Schematic diagram of the data acquisition
system.
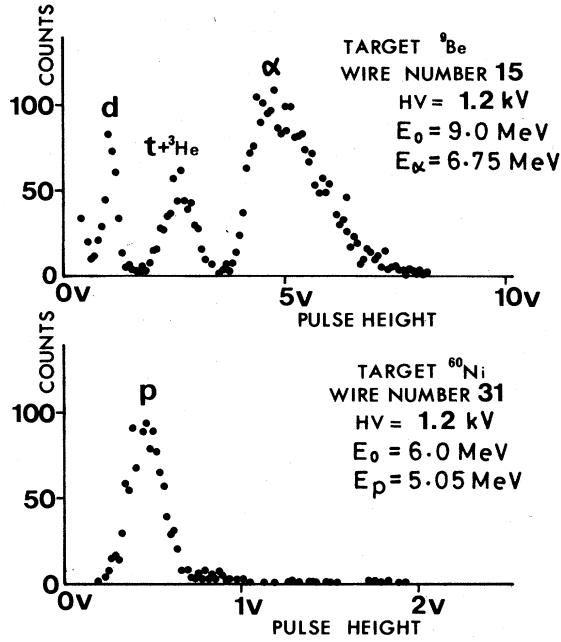
FIG. 3. Typical pulse height spectra from the MWPC.

FIG. 4. (e, α) energy spectrum of ^{90}Zr at $\theta = 90°$, for $E_e = 55$ MeV. Alpha-particle energy was corrected for energy loss in half target thickness.

$$\sigma^{(e,\alpha)}_{\lambda L}(E_e) = \text{const} \times \int_0^{E_e} \sigma^{(\gamma,\alpha)}_{\lambda L}(E_\gamma) N^{VP}_{\lambda L}(E_e, E_\gamma) dE_\gamma,$$

(2)

III. EXPERIMENTS AND RESULTS

A. (γ,α) and (γ,α_0) cross sections

The (e, α) differential cross section at 90° was measured at electron energies from 13.5 to 66.5 MeV at intervals of 0.5 MeV. Alpha particles between 6.9 and 16.8 MeV were summed after the correction for the solid angle of the detector. The result is shown in Fig. 5. The (e, α) cross section is related to the (γ, α) cross section, as follows:

$$\sigma^{(e,\alpha)}(E_e) = \sum_{\lambda L} \sigma^{(e,\alpha)}_{\lambda L}(E_e),$$

(1)

where $N^{VP}_{\lambda L}(E_e, E_\gamma)$ is the virtual photon spectrum of energy E_γ and multipolarity λL for electron energy E_e. The extraction of the (γ, α) cross section from the (e, α) cross section was done first of all on the assumption that all of the α particles are attributed to the $E1$ interaction. The ^{90}Zr(γ, α) cross section was deduced by the variable-bin Penfold-Leiss method.[39-41] $E1$ virtual photon spectra used in the analysis were calculated from the analytical expression of Nascimento et $al.$,[42] which was obtained from a fit to the distorted-wave Born approximation (DWBA) calculations of Gargaro and Onley.[43] The analysis also took into account bremsstrahlung,[44] which came from the target and from the Ti vacuum window separating the scattering chamber from the accelerator at

TABLE I. Experimental conditions.

Experiment	Electron energy (MeV)	Spectrometer angle (degree)	α-particle energy (MeV)
(e, α) cross section	13.5—66.5 (interval 0.5)	90	6.9—16.8
(γ, α_0) cross section	14.0—23.5 (interval 0.5)	90	
Multipolarity	60.0	90	6.9—10.1 10.1—11.5 11.5—13.5 13.5—16.8
Angular distributions (γ, α_0)	17.5	45—135 (interval 15)	9.3—10.3
(e, α)	40.0	45—135 (interval 15)	10.1—11.5 11.5—13.5 13.5—16.8
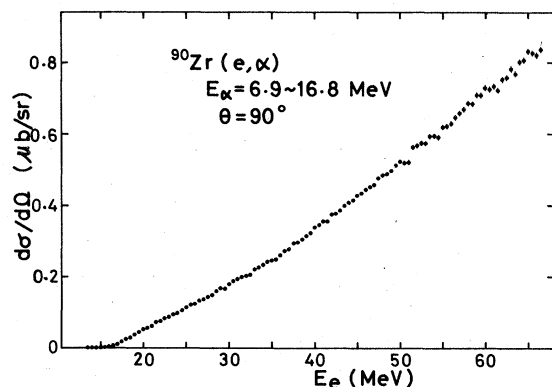
FIG. 5. Differential cross section of the (e, α) reaction at $\theta = 90°$.

the entrance of the scattering chamber.

The closed points in Fig. 6 give the (γ, α) cross section on ^{90}Zr. There is a broad bump above 30 MeV in addition to a peak at 18 MeV. The solid line in Fig. 6 is the (γ, n) cross section[45]; the position of the peak corresponds to the $T_<$ GDR, and the peak at 18 MeV in the (γ, α) cross section agrees with it.

The ^{90}Zr(γ, α_0) cross section, which is shown by the open circles in Fig. 6, was obtained from the higher energy part of the spectra measured with successive electron energies; the method is similar to that described in Ref. 46. It shows that the (γ, α_0) cross section dominates the (γ, α) cross section in the GDR region. It appears that the (γ, α_0) cross section surpasses the total (γ, α) cross section in the low energies because the
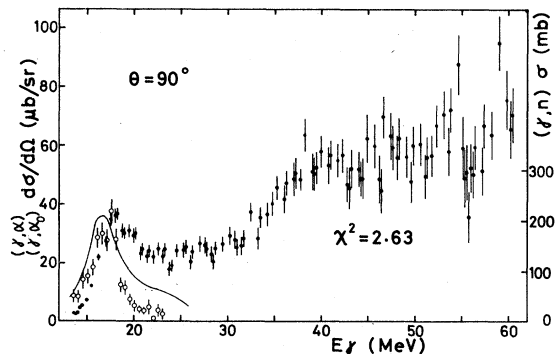
FIG. 6. Photoalpha differential cross section of ^{90}Zr (closed points) analyzed from the (e, α) cross section in Fig. 5 and ^{90}Zr(γ, α_0) differential cross section (open circles), at $\theta = 90°$. $E1$ interaction only was considered in these analyses. The value of χ^2 for the total (γ, α) cross section was calculated for the cross section smoothed by eye. Solid line shows ^{90}Zr(γ, n) cross section.
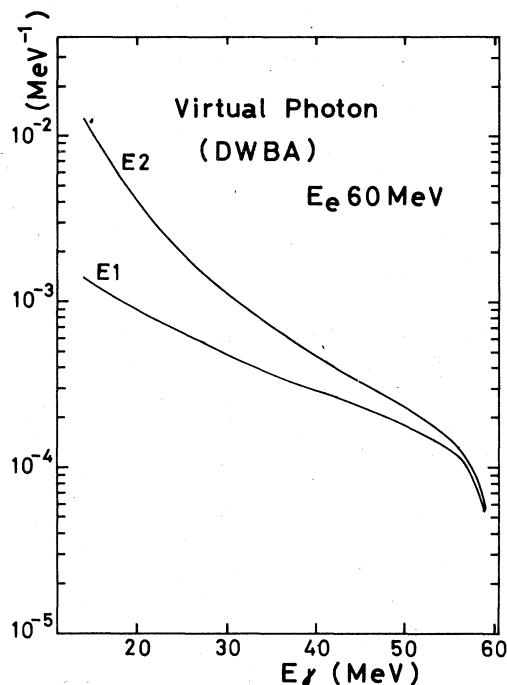
FIG. 7. Electric dipole and quadrupole virtual photon spectra for electrons of kinetic energy 60 MeV, scattered by a ^{90}Zr nucleus.

missing part of α particles due to energy loss through the target was corrected for the (γ, α_0) cross section but not corrected for the (γ, α) cross section.

In the above analyses, only the $E1$ cross section was assumed to exist over the full energy region in which the experiments were made. However, a small $E2$ contribution to the cross section might have a considerable effect on the analyses because the $E2$ component of virtual photons is much larger than the $E1$ component, as shown in Fig. 7. Two additional analyses of the total (γ, α) cross section were made taking account of the $E2$ component:

(a) both $E1$ and $E2$ cross sections in the giant resonance region,

(b) $E1$ cross section in the giant resonance region and $E2$ cross section above 30 MeV.

The (e, α) cross section was fitted by $E1$ and $E2$ (γ, α) cross sections calculated from Eqs. (1) and (2) using Lorentz shapes for the cross sections. These were slightly corrected at low energies in order to make the (e, α) cross section vanish below a cutoff energy (the cutoff energy means the lowest electron energy that gives the lowest α energy considered):

TABLE II. Parameters of Lorentz shapes.

σ_1 (μb/sr)	Γ_1 (MeV)	E_1 (MeV)	σ_2 (μb/sr)	Γ_2 (MeV)	E_2 (MeV)	E_{cut} (MeV)	C (MeV)	χ^2
(a) $E1$ and $E2$ cross sections in the giant resonance region								
7.21	6.0	18.5	16.57	6.5	16.5	13.0	3.5	18.50
(b) $E1$ cross section in the giant resonance region and $E2$ cross section above 30 MeV								
24.75	7.5	18.5	24.02	21.0	38.0	13.0	3.5	3.08

$$\sigma_{\lambda L}^{(\gamma,\alpha)}(E_\gamma) = \sigma_{\lambda L}^{(\gamma,\alpha)} \frac{E_\gamma^2 \Gamma_{\lambda L}^2}{(E_\gamma^2 - E_{\lambda L}^2)^2 + E_\gamma^2 \Gamma_{\lambda L}^2} \quad \text{for } E_\gamma > E_{cut} + C$$

$$= \frac{E_\gamma - E_{cut}}{C} \sigma_{\lambda L}^{(\gamma,\alpha)} \frac{E_\gamma^2 \Gamma_{\lambda L}^2}{(E_\gamma^2 - E_{\lambda L}^2)^2 + E_\gamma^2 \Gamma_{\lambda L}^2} \quad \text{for } E_{cut} < E_\gamma \leq E_{cut} + C$$

$$= 0 \quad \text{for } E_\gamma \leq E_{cut} . \tag{3}$$

An analytical formula by Nascimento et al.[42] was used for the $E1$ virtual photon spectrum, and the following formula for the $E2$ photon spectrum:

$$N_{E2}^{VP}(E_e, E_\gamma) = \frac{\alpha}{\pi E_\gamma} \left[\frac{E_0^2 + E^2}{p^2} \ln\left(\frac{E_0 E + pp' - m_e^2}{m_e E_\gamma}\right) + \frac{8}{3}\left(\frac{p'}{E_\gamma}\right)^2 \right] + \frac{0.69}{E_0} \exp\left[-15\left(\frac{E_\gamma}{E_0} - 0.65\right)^3 - 6.71\left(\frac{E_\gamma}{E_0}\right) \right], \tag{4}$$

where $E_0 = E_e + m_e$, $E = E_0 - E_\gamma$,

$$p = (E_0^2 - m_e^2)^{1/2}, \quad p' = (E^2 - m_e^2)^{1/2} .$$

The first term of the right-hand side in Eq. (4) is the virtual photon spectrum given by Barber,[47] and the second term is a correction term. The values of the constants in the second term were determined so that the values calculated using the equation on ^{90}Zr agree with those given by DWBA calculations. The code presented by Onley[43] was used for the calculation.

The results using a least squares method are shown in Table II, and the (γ, α) cross sections obtained are given in Fig. 8. What we must do next is to assess the three cases. This problem will be discussed in the following sections.

B. Multipolarity of the ^{90}Zr(γ,α) cross section

In order to study the reaction process in detail, the (e, α) cross section was divided into four parts with particular α-particle energies: 6.9–10.1 MeV, 10.1–11.5 MeV, 11.5–13.5 MeV, and 13.5–16.8 MeV (Fig. 9), and the (γ, α) cross sections were deduced from them on the assumption that the (γ, α) cross sections consist of

(a) $E1$ cross section over the full energy range,
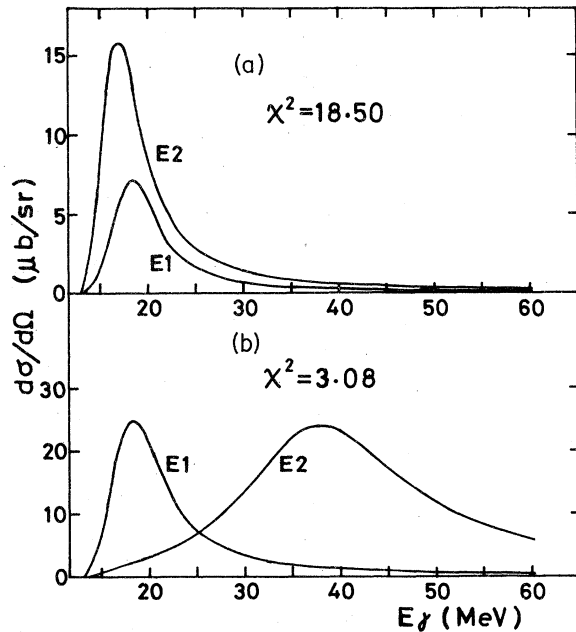
FIG. 8. Photoalpha differential cross sections reduced by taking account of the $E1$ and $E2$ components; (a) both $E1$ and $E2$ cross sections in the giant resonance region, (b) $E1$ cross section in the giant resonance region and $E2$ cross section above 30 MeV.
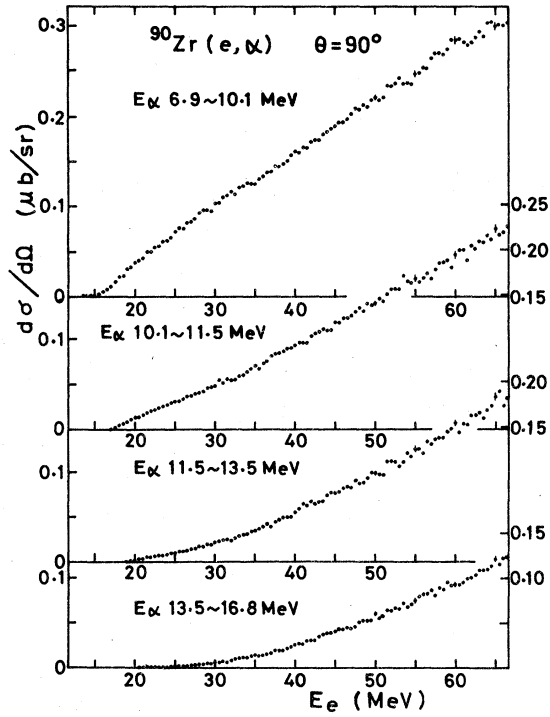
FIG. 9. ^{90}Zr(e, α) cross sections divided into four parts with particular α-particle energies.

(b) $E1$ and $E2$ cross sections in the giant resonance region,

(c) $E1$ cross section in the giant resonance region and $E2$ cross section above 30 MeV.

The method of fitting has been described in Sec. III A. The results are shown in Fig. 10 and in Table III. It was difficult to get a small χ^2 in case (b) although the parameters were changed over wide ranges. In this case, the sum of the four cross sections does not equal that shown in Fig. 8(a).

An experiment was performed to assess the three cases. Copper foils were placed in front of the ^{90}Zr target, so that the ^{90}Zr target was irradiated with bremsstrahlung from the copper foils plus electrons. The yield of α particles is given by

$$Y_{\lambda L}^{\text{TOTAL}}(E_e, t) = Y_{\lambda L}^{\text{BS}}(E_e, t) + Y_{\lambda L}^{VP}(E_e), \qquad (5)$$

$$Y^{\text{TOTAL}}(E_e, t) = \sum_{\lambda L} Y_{\lambda L}^{\text{TOTAL}}(E_e, t). \qquad (6)$$

The first term of the right-hand side in Eq. (5) shows the yield associated with bremsstrahlung, and

$$Y_{\lambda L}^{\text{BS}}(E_e, t) = \text{const} \int_0^{E_e} \sigma_{\lambda L}^{(\gamma, \alpha)}(E_\gamma) N^{\text{BS}}(E_e, t, E_\gamma) dE_\gamma, \qquad (7)$$

where $N^{\text{BS}}(E_e, t, E_\gamma)$ is the bremsstrahlung spectrum, t is the thickness of the copper foil, E_e is the electron energy, E_γ is the photon energy, and $\sigma_{\lambda L}^{(\gamma, \alpha)}(E_\gamma)$ is the (γ, α) cross section for multipolarity λL. The second term in Eq. (5) is the yield of α particles due to virtual photons of the multipolarity λL, and is given by

$$Y_{\lambda L}^{VP}(E_e) = \text{const} \times \int_0^{E_e} \sigma_{\lambda L}^{(\gamma, \alpha)}(E_\gamma) N_{\lambda L}^{VP}(E_e, E_\gamma) dE_\gamma, \qquad (8)$$

where $N_{\lambda L}^{VP}(E_e, E_\gamma)$ is the number of virtual photons with multipolarity λL and photon energy E_γ due to an electron with energy E_e.

Now we consider $P(t)$:

$$P(t) \equiv \frac{\sum_{\lambda L} Y_{\lambda L}^{\text{TOTAL}}(E_e, t)}{\sum_{\lambda L} Y_{\lambda L}^{VP}(E_e)}$$

$$= \frac{\sum_{\lambda L} \int_0^{E_e} \sigma_{\lambda L}^{(\gamma, \alpha)}(E_\gamma) N^{\text{BS}}(E_e, t, E_\gamma) dE_\gamma}{\sum_{\lambda L} \int_0^{E_e} \sigma_{\lambda L}^{(\gamma, \alpha)}(E_\gamma) N_{\lambda L}^{VP}(E_e, E_\gamma) dE_\gamma} + 1. \qquad (9)$$

The value obtained from the experiment is denoted $P_{\text{exp}}(t)$:

$$P_{\text{exp}}(t) = \frac{Y_{\text{exp}}^{\text{TOTAL}}(E_e, t)}{Y_{\text{exp}}^{VP}(E_e)}. \qquad (10)$$

As shown in Fig. 7,

$$N_{E2}^{VP}(E_e, E_\gamma) > N_{E1}^{VP}(E_e, E_\gamma), \qquad (11)$$

and $N^{\text{BS}}(E_e, t, E_\gamma)$ is the same for $E1$ and $E2$. Therefore the value of $P(t)$ for the $E1$ cross section will be greater than that for the $E2$ at the same t. The inclinations of $P(t)$ for higher multipolarities are gentler than the slope for the $E2$ because their virtual photons exceed $E2$ virtual photons. The slope for the $M1$ interaction will be close to that for the $E2$ because the $M1$ virtual photon spectrum is like the $E2$ (Refs. 43 and 47). In the case of the $E0$ interaction, the $E0$ transition with a real photon is forbidden, and the slope of $P(t)$ will be horizontal. One can decide whether the cross section is associated with the $E1$ interaction, the $E2$, or other interaction by comparing the measured and calculated $P(t)$ values.

The experiment was done with copper foils of four thicknesses: 139.3, 268.8, 399.2, and 536.6 mg/cm^2. The electron energy was 60 MeV, and emitted α particles were measured at 90° to the electron beam. Measurements were made for two values of magnetic field in the spectrometer, corresponding to α particles with $E_\alpha = 6.0$–10.5 and $E_\alpha = 9.4$–16.3 MeV. The experimental results for $P_{\text{exp}}(t)$ are shown in Fig. 11 for four ranges of α-particle energy. These have been corrected for energy loss in the target, and correspond to the
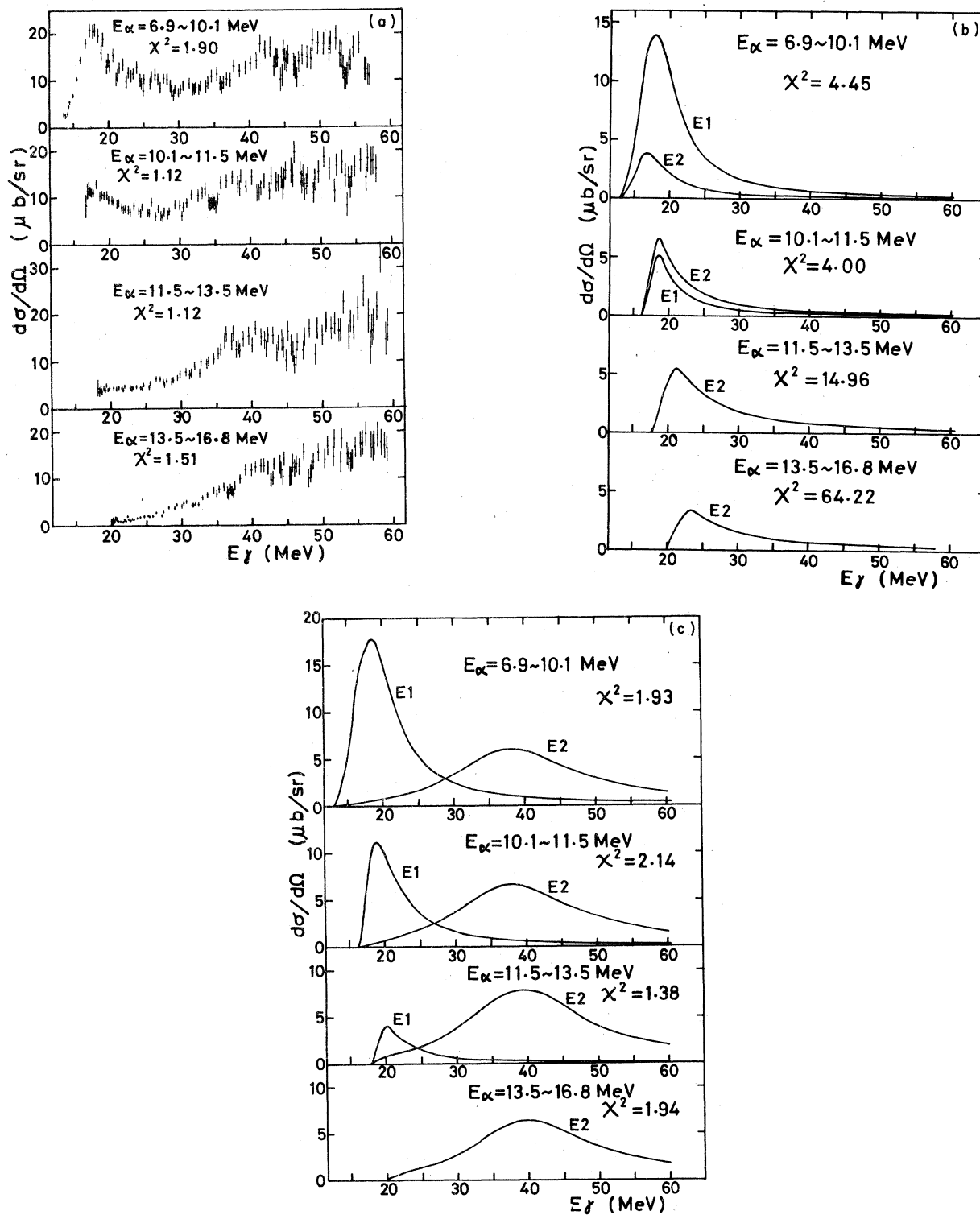
FIG. 10. ^{90}Zr(γ, α) cross sections analyzed from the (e, α) cross sections in Fig. 9. (a) An $E1$ cross section was assumed over the full energy range. The value of χ^2 was calculated for the cross sections smoothed by eye. (b) $E1$ and $E2$ cross sections were assumed in the giant resonance region. (c) An $E1$ cross section was assumed in the giant resonance region, and an $E2$ cross section above 30 MeV.

TABLE III. Parameters of Lorentz shapes.

E_α (MeV)	σ_1 ($\mu b/sr$)	Γ_1 (MeV)	E_1 (MeV)	σ_2 ($\mu b/sr$)	Γ_2 (MeV)	E_2 (MeV)	E_{cut} (MeV)	C (MeV)	χ^2
(b) $E1$ and $E2$ cross sections in the giant resonance region									
6.9—10.1	13.99	7.0	18.0	3.93	7.0	16.5	13.0	3.5	4.45
10.1—11.5	5.94	6.0	17.5	10.88	7.0	15.5	16.5	2.0	4.00
11.5—13.5	0.00	6.0	17.0	20.24	7.0	14.5	18.5	3.0	16.13
13.5—16.8	0.00	6.0	17.0	18.62	7.0	14.5	20.0	3.5	64.22
(c) $E1$ cross section in the giant resonance region and $E2$ cross section above 30 MeV									
6.9—10.1	17.61	7.5	18.5	6.07	20.0	38.0	13.0	3.0	1.93
10.1—11.5	11.65	7.5	18.5	6.60	20.0	38.0	16.5	2.0	2.14
11.5—13.5	4.85	7.5	18.5	7.79	20.0	39.0	18.5	2.0	1.38
13.5—16.8	0.00	7.5	18.5	6.41	20.0	40.0	20.0	2.0	1.94

ranges in Fig. 10. The calculated values are also shown in Fig. 11 for the $E1$ and $E2$ interactions.

In the calculation, bremsstrahlung spectra were calculated using a formula given by Schiff,[44] and virtual photon spectra by using a formula of Nascimento et al. and Eq. (4). In case (a), the (γ, α) cross sections in Fig. 10(a) were used for $\sigma_{E1}^{(\gamma, \alpha)}(E_\gamma)$ in Eq. (9) after smoothing by eye. The experimental results are very close to the values calculated on the assumption that all α particles are associated with the $E1$ interaction.
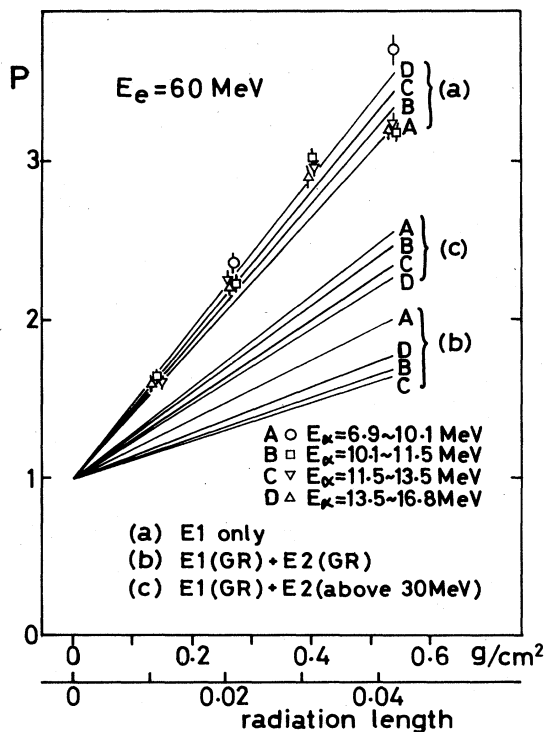
FIG. 11. Increase of α yields for thickness of brems-strahlung target (Cu). Three sets of straight lines (a), (b), (c) correspond to (a), (b), (c) in Fig. 10.

C. Angular distributions

The angular distribution of the (γ, α_0) reaction was measured at an electron energy of 17.5 MeV. The $E1$ and $E2$ cross sections were determined using the expression[31]

$$W(\theta) = \frac{1}{4\pi} [\sigma_1(1 - P_2) + \sigma_2(1 + 0.71P_2 - 1.71P_4)$$

$$- 2.68(\sigma_1\sigma_2)^{1/2} \cos\theta_{12}(P_1 - P_3)], \quad (12)$$

where σ_1 and σ_2 are the $E1$ and $E2$ cross sections, and θ_{12} is the difference in phase between α-particle waves with $l=1$ and $l=2$. The result $\sigma_2/\sigma_1 = 0.009^{+0.040}_{-0.009}$ at $\langle E_\gamma \rangle = 17.07 \pm 0.24$ MeV was obtained through the method of least squares (Fig. 12). The result shows that the $E2$ component for the ground state transition is very small and is consistent
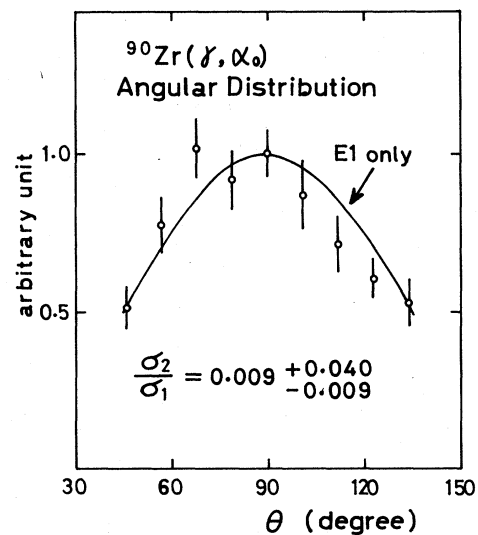
FIG. 12. Angular distribution of $^{90}Zr(\gamma, \alpha_0)$ cross section at $E_\gamma = 17.07 \pm 0.24$ MeV. A solid curve shows the calculation result for a pure $E1$ cross section.

Angular Distribution
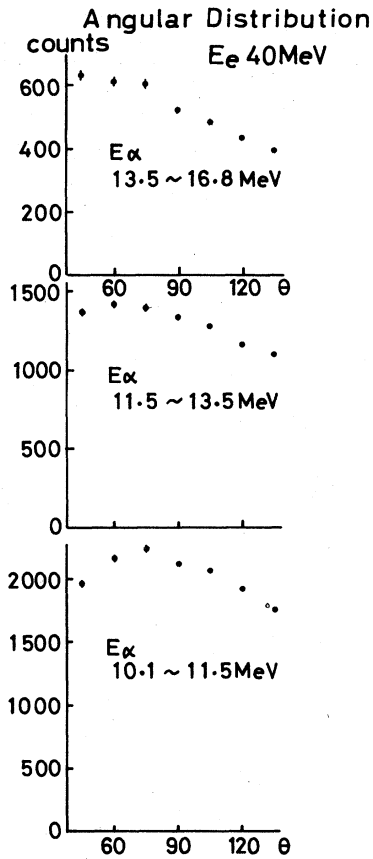
FIG. 13. Alpha-particle angular distributions at E_e =40 MeV.

with the experiment of Sec. III B.

Angular distributions of α particles from ^{90}Zr were also measured for three ranges of α-particle energy with a 40 MeV electron beam. The result is shown in Fig. 13. The angular distribution is forward-peaked for the highest α-particle energy, and more symmetric about 90° for lower α-particle energies. As shown in Sec. III B, α particles above 13.5 MeV come from the $E1$ cross section above 30 MeV, and the forward-peaked angular distribution reflects the nature of the cross section above 30 MeV. These α particles cannot be explained by a compound nucleus process because the calculation based on a statistical theory gives a symmetric angular distribution at 90°. The forward peaking obtained experimentally suggests that these α particles are emitted relatively directly from earlier stages of the reaction. Interference with a small $E2$ component also may be necessary to explain the forward-peaked angular distribution. The more symmetric angular distribution for α particles with lower energies is due

to a contribution from α particles emitted through the giant resonance [Fig. 10(a)]. As shown in Fig. 6, the (γ, α_0) cross section forms a large fraction of the (γ, α) cross section in the GDR region. The angular distribution tends to be nearly symmetric to 90° for lower α-particle energies because the angular distribution for the (γ, α_0) reaction is very similar to that of a pure $E1$ process (Fig. 12).

IV. DISCUSSION

In Secs. III B and III C, most α particles emitted through the (γ, α) reaction in ^{90}Zr are associated with the $E1$ interaction, and a broad bump exists above 30 MeV in addition to one in the GDR region. The reaction mechanism is discussed in this section.

A. Compound nucleus model

The (γ, α) cross section of ^{90}Zr has two bumps as shown in Fig. 6, one at 18 MeV corresponding to the GDR and the other above 30 MeV. In the giant resonance region, the (γ, α_0) cross section forms a major part of the (γ, α) cross section. This result is explained by the compound nucleus model. On the basis of the Hauser-Feshbach formula,[48] the (γ, α_0) cross section is expressed as

$$\sigma^{(\gamma, \alpha_0)}(E_\gamma) = \sigma^{CN}(E_\gamma) \frac{T(\alpha_0)}{\sum_c T_C}, \qquad (13)$$

where σ^{CN} is the compound nucleus formation cross section and $T(\alpha_0)$ is the transmission coefficient of the emitted α particle leading to the ground state of the residual nucleus. The denominator is the sum of the transmission coefficients for all possible decay channels.

Considering the angular distribution of the $E1$ interaction [see Eq. (12)], the differential cross section at 90° for the even-even nucleus is given by

$$\frac{d\sigma^{(\gamma, \alpha_0)}(E_\gamma)}{d\Omega} = \frac{3}{8\pi} \sigma^{CN}(E_\gamma) \frac{T(\alpha_0)}{\sum_c T_C}. \qquad (14)$$

Similarly, it is assumed that all neutrons are emitted through the compound nuclear process

$$\sigma^{(\gamma, n)}(E_\gamma) = \sigma^{CN}(E_\gamma) \frac{\sum_{c'} T_{c'}(n)}{\sum_c T_C}. \qquad (15)$$

From Eqs. (14) and (15) it follows that

$$\frac{d\sigma^{(\gamma, \alpha_0)}(E_\gamma)}{d\Omega} = \frac{3}{8\pi} \frac{T(\alpha_0)}{\sum_{c'} T_{c'}(n)} \sigma^{(\gamma, n)}(E_\gamma). \qquad (16)$$

The transmission coefficients were calculated using Woods-Saxon type optical potentials shown in Table IV, which had been obtained through the

TABLE IV. Optical potential parameters used for calculations of transmission coefficients.

	r_0 (fm)	a_0 (fm)	V_0 (MeV)	r_i (fm)	a_i (fm)	W_I (MeV)	V_{SO} (MeV)	r_C (fm)
(n)	1.25	0.65	$52.5 - 0.625E$	1.25	0.98	$5.4 + 0.4E$	$10.185 - 0.171E$	
(α)	1.553	0.631	34.63	1.553	0.631	17.35		1.4

experiments of α scattering[49] and neutron scattering.[50] On the assumption of an isotropic angular distribution for all α particles except those leading to the ground state, the (γ, α) cross section is written in the form

$$\frac{d\sigma^{(\gamma,\alpha)}(E_\gamma)}{d\Omega} = \frac{\sigma^{(\gamma,n)}(E_\gamma)}{\sum_{c'} T_{c'}(n)}\left[\frac{3}{8\pi}T(\alpha_0) + \frac{1}{4\pi}\sum_{i \neq 0}T(\alpha_i)\right].$$

(17)

The solid lines in Fig. 14 are the cross sections calculated by Eqs. (16) and (17). Both (γ, α) and (γ, α_0) cross sections calculated by this model agree well with the experimental results in the giant resonance region. However, the (γ, α) cross section above 20 MeV is not explained by this model at all.

B. Pre-equilibrium exciton model combined with the quasi-deuteron model

The angular distribution of α particles emitted from the region above 30 MeV shows a forward peaking as discussed in Sec. III C. This implies that α particles from the excited state above 30 MeV are not always emitted through a compound nuclear process.

A calculation was made in the framework of the pre-equilibrium exciton model combined with the quasi-deuteron model. The photonuclear reaction above the giant resonance region has been successfully studied on the basis of the quasi-deuteron model, which was introduced by Levinger.[17] According to this model, a photon is absorbed through the photodisintegration of a correlated neutron-proton pair in the nucleus. Levinger showed that the absorption cross section could be written as

$$\sigma_\gamma(E_\gamma) = L\frac{NZ}{A}\sigma^D(E_\gamma),$$

(18)

where σ^D is the photodisintegration cross section for a free deuteron, and L is a constant which indicates the probability of this process compared with the disintegration of a free deuteron, whose value was obtained theoretically to be 6.4. Thereafter, different values of L have been obtained ex-

perimentally by many investigators, for example $L = 2.8$ by Costa et al.[27] and $L = 10.3$ by Garvey et al.[21]

In the case of the emission of α particles on medium-weight and heavy nuclei, the (n, α) and (p, α) reactions have been successfully studied in the pre-equilibrium exciton model,[13-16] An incoming particle, having entered the nucleus, hits a particle (proton, neutron, or preformed α particle) in the nucleus, and makes a particle-hole pair. A two-particle one-hole state (so-called three exciton state) formed in this way decays either by particle emission or by a transition to a five-exciton state through an exciton-particle scattering in the nucleus.

In the case of the pre-equilibrium exciton model combined with the quasi-deuteron model, the first stage of the reaction is characterized by a four exciton state (one-particle one-hole pairs which are made for both proton and neutron through the quasi-deuteron process). An alpha particle-hole pair can be formed for the first time in the six-exciton state.

The calculation of the (γ, α) reaction can be done with the same formalism as for the (n, α) or (p, α) reaction involving the pre-equilibrium exciton mo-
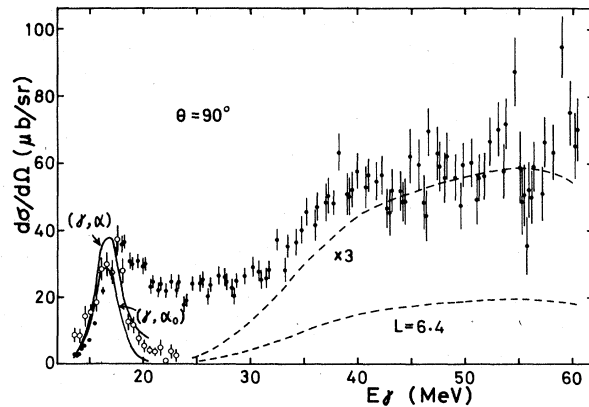
FIG. 14. Comparison of the compound nucleus model (solid lines) and the pre-equilibrium exciton model combined with the quasi-deuteron model (dashed lines) with the experimental $^{90}Zr(\gamma, \alpha)$ cross section (closed points) and $^{90}Zr(\gamma, \alpha_0)$ cross section (open circles).

del, with a slight modification:

$$\sigma^{(\gamma,\alpha)}(E) = \sigma_\gamma(E) \int \frac{m_\alpha \epsilon \sigma_{inv}(\epsilon) g_R}{4\pi^3 \hbar^2 |M|^2 g_C{}^5 E^3} \, d\epsilon$$

$$\times \sum_{\substack{n=6 \\ (\Delta n = 2)}}^{\bar{n}} \left(\frac{g_R U}{g_C E}\right)^{(n-2)}$$

$$\times (n^2 - 1) n \frac{\varphi K_{n-1}^\alpha}{\varphi K_n^\alpha + (1-\varphi)K_n^\nu} . \qquad (19)$$

Symbols in Eq. (19) are as follows:

$\sigma_\gamma(E)$ is the photon absorption cross section.

m_α and ϵ are the reduced mass of the α particle and its kinetic energy in the exit channel.

$\sigma_{inv}(\epsilon)$ is the cross section for the inverse process: the absorption cross section for an α particle with the kinetic energy ϵ.

g_R and g_C are the single particle level density in the residual and target nucleus.

U and E are the excitation energy of the residual nucleus and that of the nucleus before decay.

n is the exciton number in each stage of the cascade, which varies only by two units.

$\bar{n}$ is the exciton number of the state at equilibrium.

M is the matrix element describing the transition from a state with n excitons to the subsequent state with $n+2$.

K_n^α and K_n^ν are factors for an α particle and a nucleon introducing the corrections due to charge conservation and assuming the α particle to have a level density equal to $g/4$.

φ is the probability for the nucleon in the intranuclear cascade to strike a preformed α particle.

The inverse cross section $\sigma_{inv}(\epsilon)$ is represented by the formula

$$\sigma_{inv}(\epsilon) = \pi \lambdabar^2 \sum_l (2l+1) T_l(\epsilon)$$

$$= \frac{\pi \hbar^2}{2m_\alpha \epsilon} \sum_l (2l+1) T_l(\epsilon) , \qquad (20)$$

where $T_l(\epsilon)$ is the transmission coefficient for an α particle with kinetic energy ϵ and angular momentum l.

The following relations were also used[15,51]:

$$|M|^2 = 8A^{-3} \ (\text{MeV}^2) , \qquad (21)$$

$$g = \frac{6}{\pi^2} \frac{A}{7.5} \ (\text{MeV}^{-1}) , \qquad (22)$$

$$\bar{n} = (2Eg_C)^{1/2} . \qquad (23)$$

The photon-absorption cross section was calculated from Eq. (18) using the deuteron photodisintegration cross section σ^D presented by Partovi.[52] The parameter φ was assumed to be 0.2 (Ref. 15).

The differential cross section for the ^{90}Zr(γ,α) reaction was calculated using

$$\frac{d\sigma^{(\gamma,\alpha)}(E_\gamma)}{d\Omega} = \frac{1}{4\pi} \sigma^{(\gamma,\alpha)}(E_\gamma) . \qquad (24)$$

An isotropic angular distribution was assumed here. The calculated result is shown in Fig. 14 by a dashed line. It rises gradually with increasing excitation energy like the experimental result, although there is a slight difference in the absolute value. The value of L cannot be evaluated because the parameter φ in Eq. (19) is uncertain.

V. SUMMARY AND CONCLUSIONS

The total (e,α) cross section for ^{90}Zr and the four cross sections for particular alpha energy intervals can be described assuming a broad bump of $E1$ or $E2$ cross section above 30 MeV in addition to an $E1$ cross section in the GDR region. It is difficult to explain the (e,α) cross sections using $E1$ and $E2$ cross sections in the giant resonance region. The angular distribution of the (γ,α_0) cross section shows that the $E2$ component is not more than 1% of the $E1$ cross section at $E_\gamma = 17$ MeV. The experiment using bremsstrahlung plus electrons indicates that almost all α particles are emitted through $E1$ excitation.

The angular distribution of α particles with high energies, which are associated with the cross section above 30 MeV, shows a forward peaking. This suggests that they should be emitted through earlier stages of the reaction than a compound nuclear process.

The calculation using the pre-equilibrium exciton model combined with the quasi-deuteron model gives a bump above 30 MeV like the experimental result. Some problems in the formula by Milazzo-Colli et al. used in this paper have been pointed out.[53] They have no serious influence on the calculation made in this paper. Very recently Flowers et al.[54] and members of our group[55] have successfully compared high energy parts of α-particle spectra from the (e,α) reaction in several heavy nuclei with ones calculated by the method of Wu and Chang.[30] Their results are consistent with the existence of the (γ,α) cross section above 30 MeV.

The cross sections in the giant resonance region, both (γ,α_0) and (γ,α), can be explained by the compound nucleus model.

*Present address: National Laboratory for High Energy Physics, Oho-Machi, Tsukuba-Gun, Ibaraki-Ken, 305 Japan.

[1]M. E. Toms and J. McElhinney, Phys. Rev. 111, 561 (1958).

[2]M. Kregar and B. Povh, Phys. Lett. 2, 103 (1962).

[3]M. Kregar and B. Povh, Nucl. Phys. 43, 170 (1963).

[4]J. A. Scheer, K. Schlüpmann, and F. Triantafyllidis, Nucl. Phys. 56, 113 (1964).

[5]L. Meneghetti and S.Vitale, Nucl. Phys. 61, 316 (1965).

[6]H. Hoffmann, B. Prowe, and H. Ullrich, Nucl. Phys. 85, 631 (1966).

[7]G. Kraft, R. Kosiek, R. Mundhenke, and J. Winter, Nucl. Phys. A118, 25 (1968).

[8]P. David, J. Debrus, F. Lübke, H. Mommsen, R. Schoenmackers, and G. Stein, Nucl. Phys. A221, 145 (1974).

[9]J. J. Murphy II, H. J. Gehrhardt, and D. M. Skopik, Nucl. Phys. A277, 69 (1977).

[10]N A. Keller and D. B. McConnell, Can. J. Phys. 50, 1554 (1972).

[11]J. J. Murphy II, D. M. Skopik, J. Asai, and J. Uegaki, Phys. Rev. C 18, 736 (1978).

[12]A. G. Flowers, A. C. Shotter, D. Branford, J. C. McGeorge, and R. O. Owens, Phys. Rev. Lett. 40, 709 (1978).

[13]L. Colli-Milazzo and G. M. Marcazzan-Braga, Phys. Lett. 38B, 155 (1972).

[14]G. M. Braga-Marcazzan, L. Milazzo-Colli, and C. Signorini, Lett. Nuovo Cimento 6, 357 (1973).

[15]L. Milazzo-Colli and G. M. Braga-Marcazzan, Nucl. Phys. A210, 297 (1973).

[16]L. Milazzo-Colli, G. M. Braga-Marcazzan, M. Milazzo, and C. Signorini, Nucl. Phys. A218, 274 (1974).

[17]J. S. Levinger, Phys. Rev. 84, 43 (1951).

[18]A. C. Odian, P. C. Stein, A. Wattenberg, and B. T. Feld, Phys. Rev. 102, 837 (1956).

[19]M. Q. Barton and J. H. Smith, Phys. Rev. 110, 1143 (1958).

[20]P. C. Stein, A. C. Odian, A. Wattenberg, and R. Weinstein, Phys. Rev. 119, 348 (1960).

[21]J. Garvey, B. H. Patrick, J. G. Rutherglen, and I. L. Smith, Nucl. Phys. 70, 241 (1965).

[22]T. A. Gabriel, Phys. Rev. C 13, 240 (1976).

[23]S. Costa, L. Ferrero, and L. Pasqualini, Lett. Nuovo Cimento 1, 448 (1971).

[24]H. Schier and B. Schoch, Nucl. Phys. A229, 93 (1974).

[25]C. Whitehead, W. R. McMurray, M. J. Aitken, N. Middlemas, and C. H. Collie, Phys. Rev. 110, 941 (1958).

[26]N. N. Kaushal, E. J. Winhold, P. F. Yergin, H. A. Medicus, and R. H. Augustson, Phys. Rev. 175, 1330 (1968).

[27]T. A. Gabriel and R. G. Alsmiller Jr., Phys. Rev. 182, 1035 (1969).

[28]S. Costa, L. Ferrero, and L. Pasqualini, Lett. Nuovo Cimento 2, 665 (1971).

[29]V. S. Barashenkov, F. G. Gereghi, A. S. Iljinov, G. G. Jonsson, and V. D. Toneev, Nucl. Phys. A231, 462

(1974).

[30]J. R. Wu and C. C. Chang, Phys. Rev. C 16, 1812 (1977).

[31]L. Meyer-Schützmeister, Z. Vager, R. E. Segel, and P. P. Singh, Nucl. Phys. A108, 180 (1968).

[32]R. B. Watson, D. Branford, J. L. Black, and W. J. Caelli, Nucl. Phys. A203, 209 (1973).

[33]G. S. Foote, D. Branford, R. A. I. Bell, and R. B. Watson, Nucl. Phys. A220, 505 (1974).

[34]R. E. Peschel, J. M. Long, H. D. Shay, and D. A. Bromley, Nucl. Phys. A232, 269 (1974).

[35]G. S. Foote, D. Branford, D. C. Weisser, N. Shikazono, R. A. I. Bell, and F. C. P. Huang, Nucl. Phys. A263, 349 (1976).

[36]M. Sugawara, Proceedings of Kawatabi Conference of New Giant Resonance, Supplement to Research Report of Laboratory of Nuclear Science, Tohoku University, 8, 18 (1975).

[37]E. Wolynec, W. R. Dodge, and E. Hayward, Phys. Rev. Lett. 42, 27 (1979), and private communications.

[38]K. Shoda, M. Sugawara, T. Saito, and H. Miyase, Nucl. Phys. A221, 125 (1974).

[39]A. S. Penfold and J. E. Leiss, Phys. Rev. 114, 1332 (1959).

[40]H. H. Thies, Aust. J. Phys. 14, 174 (1961).

[41]E. Bramanis, T. K. Deague, R. S. Hicks, R. J. Hughes, E. G. Muirhead, R. H. Sambell, and R. J. J. Stewart, Nucl. Instrum. Methods 100, 59 (1972).

[42]I. C. Nascimento, E. Wolynec, and D. S. Onley, Nucl. Phys. A246, 210 (1975).

[43]W. W. Gargaro and D. S. Onley, Phys. Rev. C 4, 1032 (1971).

[44]L. I. Schiff, Phys. Rev. 83, 252 (1951).

[45]A. Lepretre, H. Beil, R. Bergere, P. Carlos, A. Veyssiere, and M. Sugawara, Nucl. Phys. A175, 609 (1971).

[46]M. Sugawara, T. Terasawa, T. Tamae, Y. Kawamura, H. Saito, and H. Tsubota, Nucl. Phys. A248, 477 (1975).

[47]W. C. Barber and T. Wiedling, Nucl. Phys. 18, 575 (1960).

[48]W. Hauser and H. Feshbach, Phys. Rev. 87, 366 (1952).

[49]F. Bjorklund and S. Fernback, Phys. Rev. 109, 1295 (1958).

[50]C. M. Perey and G. Perey, At. Data Nucl. Data Tables 17, 87 (1976).

[51]G. M. Braga-Marcazzan, E. Gadioli-Erba, L. Milazzo-Colli, and P. G. Sona, Phys. Rev. C 6, 1398 (1972).

[52]F. Partovi, Ann. Phys. (N.Y.) 27, 79 (1964).

[53]P. Obložinský, Phys. Lett. 74B, 6 (1978).

[54]A. G. Flowers, D. Branford, J. C. McGeorge, A. C. Shotter, P. Thorley, C. H. Zimmerman, R. O. Owens, and J. S. Pringle, Phys. Rev. Lett. 43, 323 (1979).

[55]T. Urano, M. Hirooka, and M. Sugawara, International Conference on Nuclear Physics with Electromagnetic Interactions, Abstracts of Contributed Papers, Mainz, 1979, 4.33.